7.7% Efficient All-Polymer Solar Cells

*Ye-Jin Hwang, Brett A. E. Courtright, Amy S. Ferreira, Sarah H. Tolbert, and Samson A. Jenekhe**

All-polymer solar cells, in which both the donor and acceptor materials that absorb light and transport charges are semiconducting polymers, have a great potential to replace fullerene/polymer devices.[1] Although considerable progress has been made in advancing the performance of polymer solar cells by using fullerene-based electron acceptors, with single-junction power conversion efficiencies (PCEs) of over 9%,[2] the use of n-type semiconducting polymers as acceptors has potential to overcome the high cost, poor thermal/photochemical stability, limited light absorption in the visible–near infrared region, and other limitations of fullerene derivatives.[3] Among the various n-type semiconducting polymers investigated as electron acceptors in all-polymer bulk heterojunction (BHJ) solar cells to date,[4–6] perylene diimide (PDI)-arylene[5] and nanphthalene diimide (NDI)-arylene[6] copolymers have emerged as the most promising. However, the performance of all-polymer solar cells composed of low band gap donor conjugated polymers and NDI- or PDI-based n-type semiconducting polymers has so far remained significantly lower than the corresponding fullerene/polymer devices. The main limitations of the PCE of all-polymer solar cells reported to date (≈5%–6%) are the generally low short-circuit current (≤14 mA cm^{-2}) and low fill factor (≤50%–60%) compared to fullerene/polymer devices.[5,6] Overcoming the limitations of current all-polymer BHJ devices requires exploration of new donor/acceptor polymer/polymer blend systems and blend processing strategies toward more optimal light harvesting, blend morphology, charge photogeneration, and bulk electron and hole mobilities.

Diverse methods have been successfully used for controlling the morphology of fullerene/polymer BHJ devices, including thermal annealing,[7] solvent vapor annealing,[8] self-assembly of polymer nanowires,[9] and use of processing additives.[10] These approaches have also been explored to varying degrees in polymer/polymer blend systems.[4–6] However, the self-organization behavior of polymer/polymer blends can be expected to be very different from that of the corresponding fullerene/polymer blends owing to the difference in molecular geometry of fullerene acceptors (spherical nanoparticles) and n-type semiconducting polymer acceptors (linear semiflexible/semirigid chains). The self-organization kinetics and morphology of polymer/polymer blend films processed from solution could be influenced by factors such as the solvent, solubilities of both polymers, crystalline or amorphous nature of each polymer, molecular weight, glass and/or melt transitions of both polymers, flexibility/rigidity of the chains, miscibility of the polymers, and chain entanglements.[11] Most of these factors are largely fixed for a given polymer/polymer blend solution being processed into thin films, and thus the blend self-organization rate and subsequent blend morphology will be dominated by the postdeposition annealing temperature and solvent evaporation rate from a spin-coated wet film.

In this Communication, we report high-performance all-polymer solar cells with record 7.7% power conversion efficiency, record short-circuit current density (18.8 mA cm^{-2}) and 85% peak external quantum efficiency. We show that solvent evaporation rate and self-organization of the polymer/polymer blend films, composed of a high-mobility crystalline naphthalene diimide (NDI)-selenophene copolymer acceptor (PNDIS-HD) and small band gap benzodithiophene (BDT)-thieno[3,4-*b*]thiophene (TT) copolymer donor (PBDTT-FTTE), can be controlled by film aging at room temperature and leads to a twofold enhancement in efficiency compared to the thermally (175 °C) annealed devices. The slower self-organization of polymer/polymer blends facilitated by room temperature film aging results in enhanced electron mobility as well as a more favorable bulk morphology as observed by photoluminescence (PL) quenching analysis and grazing incidence wide-angle X-ray scattering (GIWAXS) studies. We note that the performance of these all-polymer (PNDIS-HD:PBDTT-FTTE) blend solar cells is currently limited by the fill factor (≈50%), which is largely caused by a significant imbalance in charge carrier mobilities and high bimolecular recombination. Indeed, the observed short-circuit current density (18.8 mA cm^{-2}) and EQE (85%) are superior to values reported for the corresponding $PC_{71}BM$/PBDTT-FTTE solar cells.[2c,12] Power conversion efficiencies exceeding 10% can thus be expected in the n-type polymer:PBDTT-FTTE (all-polymer) blend solar cells if fill factors exceeding 65%–70% could be achieved as observed in the $PC_{71}BM$ devices.[2c,12]

The naphthalene diimide (NDI)-selenophene copolymer acceptor, PNDIS-HD, was synthesized and purified following our previous report;[6b] the PNDIS-HD sample has a weight average molecular weight (M_w) of 42.6 kDa with a polydispersity index (PDI) of 1.5. The donor polymer, PBDTT-FTTE (M_n > 25 kDa, PDI = 1.8–2.2), was purchased from Solarmer Energy, Inc. and was used as received. The molecular and electronic structures of PNDIS-HD and PBDTT-FTTE polymers are shown in **Figure 1**a,b, respectively. PNDIS-HD has a low lying lowest unoccupied molecular orbital (LUMO)

Y.-J. Hwang, B. A. E. Courtright, Prof. S. A. Jenekhe
Department of Chemical Engineering
and Department of Chemistry
University of Washington
Seattle, WA 98195-1750, USA
E-mail: jenekhe@u.washington.edu
A. S. Ferreira, Prof. S. H. Tolbert
Department of Chemistry and Biochemistry
and Department of Materials Science and Engineering
The California NanoSystems Institute
University of California
Los Angeles, Los Angeles, CA 90095-1569, USA

DOI: 10.1002/adma.201501604

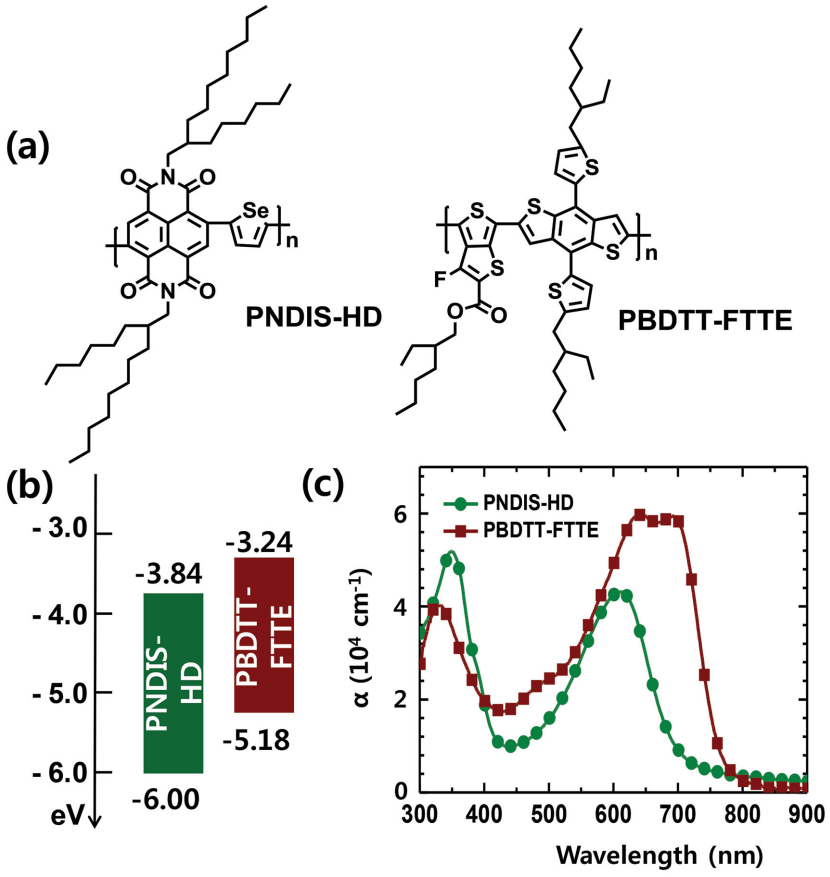

Figure 1. a) Molecular structures of acceptor polymer (PNDIS-HD) and donor polymer (PBDTT-FTTE). b) HOMO/LUMO energy levels of the acceptor and donor polymers. c) Optical absorption spectra of the acceptor and donor polymers.

energy level, with an energy of –3.84 eV relative to vacuum, as determined from the onset reduction potential (–0.8 eV vs SCE) in cyclic voltammetry (CV). CV scans up to 2 V (vs SCE) did not show an oxidation wave due to its weak electron donating nature. We thus expect the highest occupied molecular orbital (HOMO) energy level of PNDIS-HD to be either at or lower lying than –6.0 eV. This is reasonable, considering that a HOMO energy level of –5.95 eV was observed for NDI-biselenophene copolymer.[6a,13] We measured the HOMO/LUMO energy levels of PBDTT-FTTE to be –5.18/–3.24 eV (Figure S1, Supporting Information). The energy level offsets versus PNDIS-HD is thus ideal for efficient photoinduced electron and hole transfer. The thin film optical absorption spectra of both PNDIS-HD and PBDTT-FTTE (Figure 1c) reveal optical band gaps (E_g^{opt}) of 1.76 and 1.59 eV, respectively. Two distinct absorption bands centered at 350 nm with a maximum absorption coefficient (α_{max}) of 5.09×10^4 cm^{-1} and centered at 609 nm with a α_{max} of 4.32×10^4 cm^{-1} in PNDIS-HD corresponding to the π–π^* or n–π^* transition band and an intramolecular charge transfer (ICT) band,[14] respectively, were observed. The absorption bands of PBDTT-FTTE are mostly overlapped with those of PNDIS-HD, except in the near IR region where PBDTT-FTTE extends light harvesting up to 800 nm with a higher α_{max} of 5.98×10^4 cm^{-1} at 645 nm compared to those of PNDIS-HD.

Polymer/polymer BHJ solar cells based on PNDIS-HD:PBDTT-FTTE (1:1 w/w) active layer were fabricated with the inverted device structure of ITO/ZnO/PEI/active layer/MoO_3/Ag and tested under 100 mW cm^{-2} air mass 1.5 global (AM 1.5 G) solar illumination in ambient air, using poly(ethylenimine) (PEI) as a cathode interlayer. The active layer spin-coated from chlorobenzene (CB) solution was either (i) thermally annealed at 175 °C for 10 min (fast solvent evaporation), which is the most common annealing process in OPVs, or (ii) placed in an argon-filled glove box to dry at room temperature (25–28 °C) for 72 h (3 d) to facilitate slow solvent evaporation and slow blend film self-organization. The current density–voltage (J–V) curves and the external quantum efficiency (EQE) spectra are shown in **Figure 2**a,b, respectively, and the photovoltaic properties are summarized in **Table 1**.

The thermally annealed devices have an average power conversion efficiency of 3.53% while the maximum PCE is 3.66% with a short-circuit current density (J_{sc}) of 12.64 mA cm^{-2}, open circuit voltage (V_{oc}) of 0.74 V, and a fill factor (FF) of 0.39. However, the photovoltaic properties of PNDIS-HD:PBDTT-FTTE solar cells where the active layers were dried at room temperature for 72 h (3 d) have dramatically enhanced photovoltaic properties. These slowly dried devices have an average PCE of 7.21% with a maximum PCE of 7.73%, J_{sc} of 18.80 mA cm^{-2}, V_{oc} of 0.81 V, and FF of 0.51 (Table 1). Clearly, by slowing the solvent evaporation rate and thereby facilitating the gradual self-organization or phase separation of the PNDIS-HD:PBDTT-FTTE blend system, performance of the photovoltaic devices is substantially improved. First, we note that both of the observed short-circuit current and PCE of these film-aged PNDIS-HD:PBDTT-FTTE blends are the highest values reported to date for all-polymer solar cells. Second, it is also noteworthy that the observed short-circuit current density of 18.80 mA cm^{-2} (average J_{sc} = 18.61 ± 0.21 mA cm^{-2}) is even higher compared to the high performance $PC_{71}BM$:PBDTT-FTTE devices (J_{sc} = 14.02–17.24 mA cm^{-2}) with power conversion efficiencies of up to 10.3%.[2c,12] Third, it is clear that the observed FF value of 51% for the present PNDIS-HD:PBDTT-FTTE blend solar cells is substantially lower than the reported 64%–74% for the corresponding $PC_{71}BM$:PBDTT-FTTE devices,[11] which suggests that the fill factor is the primary factor limiting the photovoltaic efficiency of the present all-polymer solar cells.

The external quantum efficiency (EQE) spectra of the best PNDIS-HD:PBDTT-FTTE blend devices are shown in Figure 2b. For both thermally (175 °C) annealed and room temperature film-aged devices, the photoresponse starts at 800 nm due to the smaller optical band gap of the donor polymer. The EQE of the thermally annealed device peaks at 60% in the 580–700 nm region. In contrast, the EQE of the room

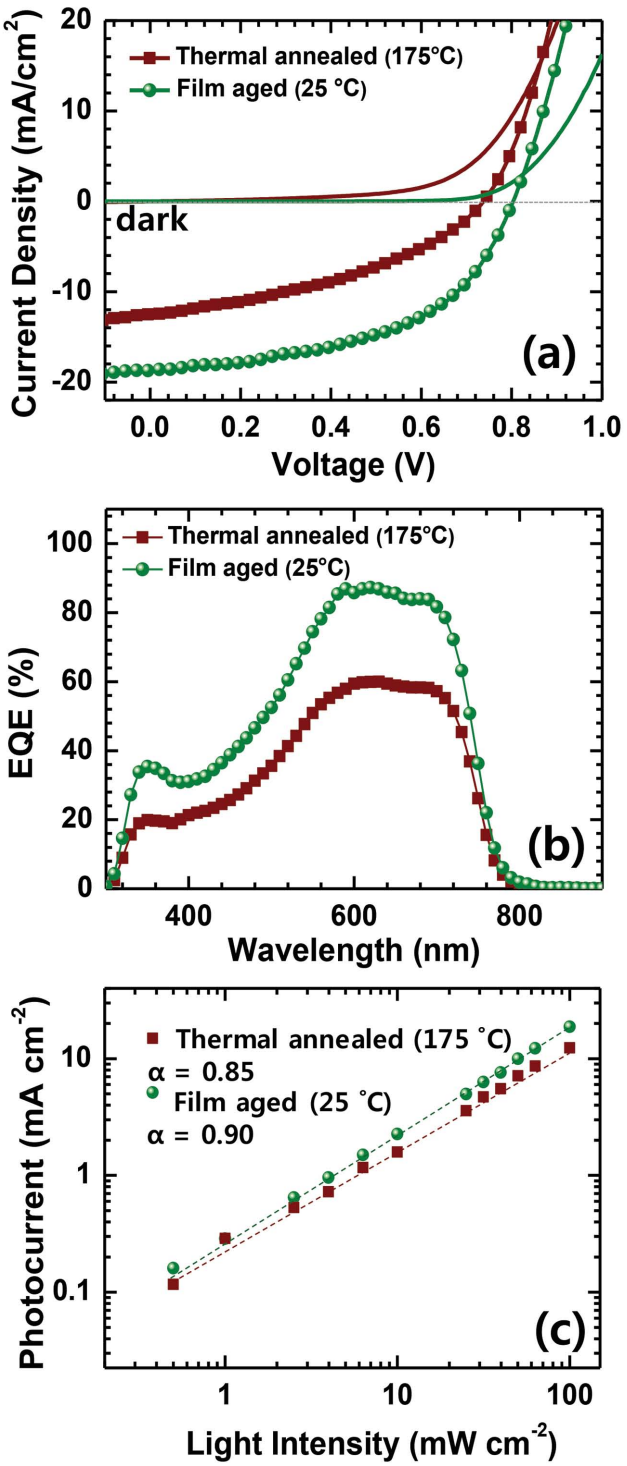

Figure 2. Current density–voltage (*J–V*) curves a) and external quantum efficiency (EQE) spectra b) of PNDIS-HD:PBDTT-FTTE (1:1 w/w) blend solar cells with thermally annealed (175 °C, 10 min) or film-aged (25 °C, 72 h) active layer. c) Short-circuit current density (J_{sc}) versus light intensity (P_{light}) data and power-law ($J_{sc} \propto P_{Light}^{\alpha}$) fit for PNDIS-HD:PBTT-FTTE solar cells.

temperature film-aged device rises to a maximum of 85% in the 580–700 nm range and remains over 50% in the 500–750 nm range, where the optical absorption bands of the donor and acceptor polymers are overlapped. This indicates that both photoinduced electron and hole transfer are efficiently contributing to charge photogeneration.[15] The short-circuit current density (J_{sc}) values calculated from the EQE spectra (11.18 mA cm^{-2} for thermally annealed devices and 16.81 mA cm^{-2} for film-aged devices) were lower than the J_{sc} values directly measured from the *J–V* curves (Figure 2a), and the mismatch between the two values was within 10%. This mismatch could be due to the initial degradation of the performance under ambient condition as well as the spectral mismatch between the simulated light source and the AM1.5 G solar spectrum. The much lower EQE in the 300–500 nm is also a major factor in the loss in efficiency of the present all-polymer solar cells compared to the corresponding $PC_{71}BM$:PBDTT-FTTE devices (Figure S5, Supporting Information).

Short-circuit current as a function of illumination intensity (P_{light}) in thermally annealed and film-aged PNDIS-HD:PBDTT-FTTE blend photodiodes was measured to understand charge recombination kinetics in the devices (Figure 2c). The J_{sc} was measured and averaged for three devices at each of 12 different light intensities, which were varied from 100 to 0.5 mW cm^{-2} by using neutral density filters. In general, J_{sc} has a power-law dependence on P_{Light} ($J_{sc} \propto P_{Light}^{\alpha}$), and linearity ($\alpha \approx 1$) indicates weak charge carrier losses due to bimolecular recombination.[16] The observed power-law exponent (α) was 0.85 for the thermally annealed devices and 0.90 for the film-aged devices. Although $\alpha < 1$ in both thermally annealed and film-aged PNDIS-HD:PBDTT-FTTE blend devices means that there is a significant amount of bimolecular recombination, the results indicate less recombination in the aged-film devices. This result can partially explain the lower fill factor (39%) in the thermally annealed solar cells with high series resistance (R_S) of 15.25 Ω cm^2 and low shunt resistance (R_{SH}) of 167.95 Ω cm^2 compared to those seen in the film-aged solar cells (FF = 51%, R_S = 8.13 Ω cm^2, R_{SH} = 239.38 Ω cm^2) (Table 1).

The bulk charge transport properties of the active layer can provide insight into the photovoltaic properties of the polymer/polymer blend solar cells, including the fill factor which depends on the carrier sweep-out rate relative to bimolecular charge recombination rate.[7] The bulk electron and hole mobilities of the PNDIS-HD:PBDTT-FTTE blend system were measured by using the space charge limited current (SCLC) method. The SCLC device structures for electron-only and hole-only measurements were ITO/ZnO/PEI/active layer/LiF/Al and ITO/PEDOT:PSS/active layer/Au, respectively. The measured *J–V* curves and Mott–Gurney equation fitting of the data are shown in **Figure 3** for the two processing conditions: thermally (175 °C) annealed and room-temperature (25 °C) film-aged. The hole mobility (μ_h) of the donor polymer (PBDTT-FTTE) in the thermally annealed blends is 2.74 × 10^{-4} cm^2 V^{-1} s^{-1}, which is essentially the same as in the room-temperature film-aged blends (3.11 × 10^{-4} cm^2 V^{-1} s^{-1}). This hole mobility value is also very comparable to μ_h values reported for other polymer:PBDTT-FTTE[6e] and $PC_{71}BM$:PBDTT-FTTE[2c,12] blends. In contrast, the bulk electron mobility in the PNDIS-HD:PBDTT-FTTE blends is found to increase threefold from 2.37 × 10^{-3} cm^2 V^{-1} s^{-1} in the thermally annealed blend films to 7.25 × 10^{-3} cm^2 V^{-1} s^{-1} in the room-temperature film-aged blends. It is important to note that the observed hole mobilities

Table 1. Photovoltaic properties of PNDIS-HD:PBDTT-FTTE blend solar cells.

Processing condition[a)]	J_{sc} [mA cm^{-2}][b)]	V_{oc} [V]	FF	PCE [%]	R_S [Ω cm^2]	R_{SH}[c)] [Ω cm^2]
175 °C, 10 min	*12.64* (12.16 ± 0.41)	*0.74* (0.73 ± 0.01)	*0.39* (0.39 ± 0.01)	*3.66* (3.53 ± 0.12)	15.25	167.95
25 °C, 72 h	*18.80* (18.61 ± 0.21)	*0.81* (0.80 ± 0.00)	*0.51* (0.48 ± 0.01)	*7.73* (7.21 ± 0.24)	8.12	239.38

[a)]Spin-coated active layer drying condition; [b)]The photovoltaic properties were averaged over 20 devices. The values in italic are the photovoltaic parameters of solar cells with the highest PCEs; [c)]The shunt resistances were extracted from the slope at 0 V of *J–V* curves in the range of –0.1–0.1 V.

in both cases are about one order of magnitude lower than the electron mobilities, and there is thus significant imbalanced bulk charge transport in both thermally annealed (μ_h/μ_e = 0.115) and film-aged blend devices (μ_h/μ_e = 0.043). Although the higher electron mobility in the film-aged blend solar cells leads to the enhanced fill factor (FF = 0.48) of these devices relative to those annealed at 175 °C (FF = 0.39),[17] the fill factor of these devices is still much lower than the corresponding fullerene/polymer photodiodes (FF > 0.6).[2c,12] This result suggests that the bulk hole transport properties of PNDIS-HD:PBDTT-FTTE blend system remain to be fully optimized for balanced bulk charge transport and advances in this area could substantially improve the FF and thus efficiency of these all-polymer BHJ solar cells.

We performed photoluminescence (PL) quenching experiments to gain insight into the nanoscale morphology and molecular miscibility of the polymer/polymer blends. The PL spectra of PBDTT-FTTE film and PNDIS-HD:PBDTT-FTTE (1:1 w/w) blend films under the two different film-forming conditions (thermally annealed and room-temperature film-aged) were measured and the PL quenching rate was calculated by integrating the PL spectra. The PL spectra when excited with Xe flash lamp at a wavelength of 645 nm are shown in **Figure 4**. PL emission band of PBDTT-FTTE was found in the range of 670–860 nm with a peak at 750 nm. The PL spectrum of the blend films was quenched 92% in the film-aged blend films compared to 78% in the thermally annealed blend films. This indicates that more efficient charge transfer occurs in the film-aged blend films due to the existence of smaller phase-separated domain sizes and/or greater molecular miscibility in the film-aged blend films than in the thermally annealed blend films. This result is also consistent with the X-ray diffraction

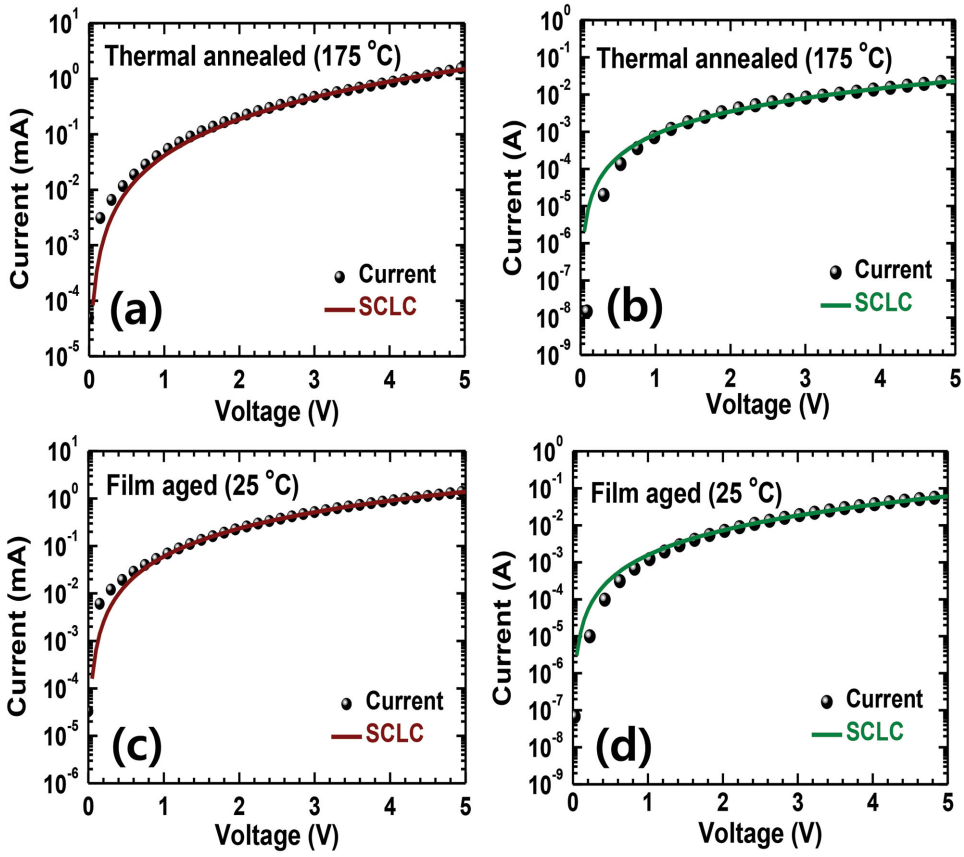

Figure 3. Space-charge-limited current (SCLC) fittings of thermally annealed devices a,b) and film-aged devices c,d) measured in ambient conditions. Electron-only SCLC devices a,c): ITO/ZnO/PEI/blend/LiF/Al and hole-only SCLC devices b,d): ITO/PEDOT:PSS/blend/Au.

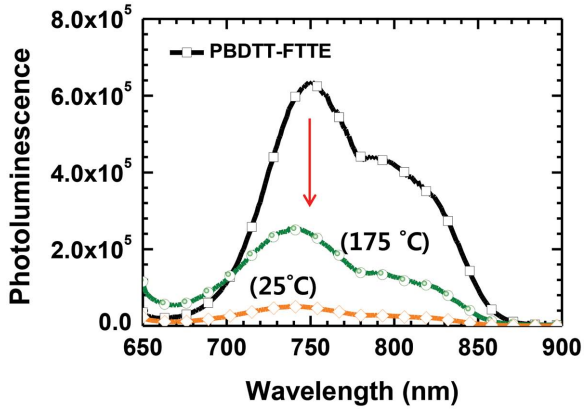

Figure 4. Photoluminescence (PL) spectra of PBDTT-FTTE film (open square) and the PBDTT-FTTE:PNDIS-HD blend films after thermal annealing at 175 °C (open circle) and after film aging at room temperature (open diamond). The excitation wavelength was 645 nm.

analysis (Figure S6, Table S1, Supporting Information) that showed smaller mean crystalline domain sizes in the film-aged blend films (6.38 nm) compared to the thermally annealed blend films (7.69 nm) calculated using the Scherrer equation.[18] However, no significant difference was observed by bright field transmission electron microscopy (TEM) imaging of the thermally annealed and film-aged blend films (Figure S3, Supporting Information). We also note that there is a possibility of vertical phase separation in the blend films due to surface energy differences in PBDTT-FTTE and PNDIS-HD as found from the difference in water contact angle ($\theta = 104.8°$ in PBDTT-FTTE and $\theta = 110.6°$ in PNDIS-HD).[19]

Grazing incidence wide-angle X-ray scattering (GIWAXS) analysis gives further insight into the morphology of the pure polymer films and the BHJ blend films (**Figure 5**). By looking at both the in-plane and out-of-plane directions of the 2D diffractograms, as shown in Figure 5c,d, the molecular orientations of the polymers in the films were determined. In the neat PBDTT-FTTE films, the polymer adopts a face-on orientation with a strong π–π interaction, as seen from the large out-of-plane (010) peak centered at about 1.5 Å^{-1}. Neat films of PNDIS-HD also showed a face-on orientation, with very strong lamellar packing peaks observed in the in-plane direction. These films exhibit a shift in the *d*-spacing, and a peak broadening of the lamellar (100) peak in the out-of-plane direction, however, indicating some edge-on polymer chains with less ordered lamellar stacking. When we turn to PNDIS-HD:PBDTT-FTTE blend films, a shift of the lamellar peak to larger *d*-spacing was observed in both the thermally annealed and the film-aged blend films, indicating that some mixing of the two polymers disorders the face-on stacking in the blend films. In the film-aged blend film, a much lower peak intensity with a larger peak shift (0.7–0.9 Å) was observed compared to the thermally annealed films (0.4–0.5 Å). This indicates the existence of more amorphous mixed regions in the film-aged blend films, compared with thermally annealed samples (Table S1, Supporting Information). Moreover, a strong lamellar peak in the out-of-plane direction of thermally annealed blend films indicates more edge-on oriented regions compared to the film-aged blend film. From this result, we conclude that slow self-organization or crystallization process by room temperature film aging produces a more favorable bulk morphology with more mixed regions to facilitate charge separation and less edge-on oriented

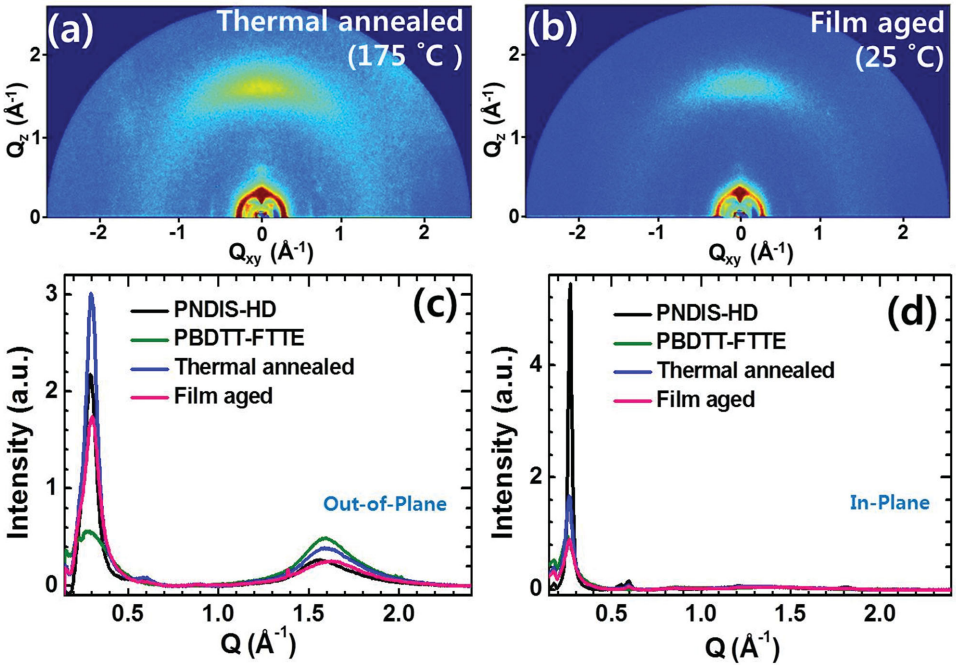

Figure 5. Grazing incidence wide-angle X-ray scattering (GIWAXS) patterns of thermally annealed (175 °C, 10 min) a) or film-aged (25 °C, 72 h) b) PNDIS-HD:PBDTT-FTTE (1:1 w/w) blend films. Line cut of GIWAXS images in the out-of-plane c) and in-plane d) of neat polymer films of PNDIS-HD and PBDTT-FTTE, and their 1:1 w/w blend films.

polymer chains to facilitate carrier mobility through the film. Both are favorable for photovoltaic applications.

In conclusion, we have demonstrated that high-performance all-polymer solar cells can be achieved by employing suitable donor and acceptor polymers and by controlling the polymer/polymer blend film self-organization rate through a simple film aging process at room temperature. The resulting all-polymer (PNDIS-HD:PBDTT-FTTE) blend solar cells combined a record 7.7% PCE and 18.8 mA cm^{-2} short-circuit current density with an EQE of 85%. The observed photovoltaic performance of the film-aged polymer/polymer blend solar cells is about two-fold enhanced compared with the related thermally (175 °C) annealed devices, which could be explained by the slower solvent evaporation rate enabled improvement in electron mobility and the favorable bulk morphology. The observed very high bulk electron mobility in these all-polymer blend devices suggests that even higher photocurrents are possible depending on a matching high-mobility donor polymer component. Our finding that the photocurrent of PNDIS-HD:PBDTT-FTTE BHJ devices is superior, whereas their fill factors are much lower compared to those of $PC_{71}BM$:PBDTT-FTTE solar cells, suggests that further optimization of materials and device engineering to achieve higher fill factors will enable the efficiency of all-polymer solar cells to exceed 10%.

Experimental Section

Materials: PNDIS-HD was synthesized according to the known literature procedures.[6b] PBDTT-FTTE (PTB7-Th, M_n > 25 kDa, PDI = 1.8–2.2) was purchased from Solarmer Energy, Inc., and used as received. ZnO precursor solution was prepared by dissolving 1 g of zinc acetate dihydrate (99.999% trace metals basis, Aldrich) in 10 mL of 2-methoxyethanol (99.8%, anhydrous, Aldrich) with 0.28 g of ethanolamine (≥99.5%, Aldrich) as a surfactant and stirring overnight under ambient conditions.

Fabrication and Characterization of All-Polymer Solar Cells: ITO glass substrate was cleaned sequentially in ultrasonic baths with acetone and isopropyl alcohol for 30 min, dried using air duster, and stored in vacuum oven. The ITO glass substrate was O_2 plasma treated for 90 s right before coating the ZnO layer. The ZnO precursor solution was spin-coated onto the ITO glass at 5000 rpm for 40 s, annealed at 250 °C on a hot plate in air for 1 h to make 20–30 nm thick ZnO layer. A 0.05 wt% polyethylenimine (PEI, $M_w \approx 25\,000$, Aldrich 408727) in 2-methoxyethanol solution was spin-coated onto the ZnO layer and dried at 110 °C on a hot plate in air for 10 min and the glass/ITO/ZnO/PEI substrate was transferred into an argon-filled glove box. Active layer (e.g., PNDIS-HD:PBDTT-FTTE blend (1:1 w/w)) solution in chlorobenzene was spin-coated at 1000 rpm for 20 s. After spin-coating, the wet film was either thermally annealed at 175 °C for 10 min or film-aged inside the glove box for 72 h (3 d) followed by thermal vacuum deposition of MoO_3 (7.5 nm) and Ag anode (100 nm). All the active layers had thicknesses of 115 ± 7 nm. Five pixels, each with an active area of 4 mm^2, were fabricated per ITO substrate. The photovoltaic cells were tested under AM 1.5 G solar illumination at 100 mW cm^{-2} in ambient condition using a Solar Simulator (model 16S, Solar Light Co., Philadelphia, PA) with a 200 W Xenon Lamp Power Supply (Model XPS 200, Solar Light Co., Philadelphia, PA) calibrated by NREL certified Si photodiode (Model 1787-04, Hamamatsu Photonics K.K., Japan) and a HP4155A semiconductor parameter analyzer (Yokogawa Hewlett-Packard, Japan). After the *J–V* measurement, the external quantum efficiency (EQE) was measured by using a solar cell quantum efficiency measurement system (Model QEX10, PV Measurements, Inc., Boulder, CO) with a 2 mm^2 (2 mm × 1 mm) size masked incident light source and TF Mini Super measurement apparatus for multiple devices in a single substrate. The EQE system was calibrated with a Si photodiode before measurement. Current–voltage (*J–V*) characteristics of the space-charge-limited current (SCLC) devices were measured by using a HP4155A semiconductor parameter analyzer (Yokogawa Hewlett-Packard, Tokyo) in dark ambient conditions. Grazing incidence wide-angle X-ray scattering (GIWAXS) was performed at the Stanford Synchrotron Radiation Lightsource (SSRL) on beamline 11-3 using a wavelength of 0.942 Å and sample-to-detector distance of 400 mm. Samples were prepared using all of the same processing methods described above with the difference being that the active layer was spun onto silicon, rather than ITO substrates.

Supporting Information

Supporting Information is available from the Wiley Online Library or from the author.

Acknowledgements

This work was supported by the NSF (DMR-1409687) and in part by the Office of Naval Research (N00014-11-1-0317). Structural studies were supported by the National Science Foundation Under Grant CHE-1112569 and in part by the Department of Energy through an EFRC program on Molecularly Engineered Energy Materials (MEEM), Grant No. DE-SC0001342. The X-ray diffraction studies presented in this manuscript were carried out at the Stanford Synchrotron Radiation Lightsource. Use of the Stanford Synchrotron Radiation Lightsource, SLAC National Accelerator Laboratory, was supported by the U.S. Department of Energy, Office of Science, Office of Basic Energy Sciences, under Contract DE-AC02-76SF00515.

Received: April 3, 2015
Revised: June 4, 2015
Published online: July 2, 2015

[1] a) J. J. M. Halls, C. A. Walsh, N. C. Greenham, E. A. Marseglia, R. H. Friend, S. C. Moratti, A. B. Holmes, *Nature* **1995**, *376*, 498; b) S. A. Jenekhe, S. J. Yi, *Appl. Phys. Lett.* **2000**, *77*, 2635; c) J. E. Anthony, A. Facchetti, M. Heeney, S. R. Marder, X. Zhan, *Adv. Mater.* **2010**, *22*, 3876; d) M. M. Alam, S. A. Jenekhe, *Chem. Mater.* **2004**, *16*, 4647; e) A. Facchetti, *Mater. Today* **2013**, *16*, 123.

[2] a) C. E. Small, S. Chen, J. Subbiah, C. M. Amb, S. W. Tsang, T. H. Lai, J. R. Reynolds, F. So, *Nat. Photon.* **2012**, *6*, 115; b) Z. He, C. Zhong, S. Su, M. Xu, H. Wu, Y. Cao, *Nat. Photon.* **2012**, *6*, 591; c) S. H. Liao, H. J. Jhuo, Y. S. Cheng, S. A. Chen, *Adv. Mater.* **2013**, *25*, 4766.

[3] a) E. Ahmed, G. Ren, F. S. Kim, E. C. Hollenbeck, S. A. Jenekhe, *Chem. Mater.* **2011**, *23*, 4563; b) H. Li, T. Earmme, G. Ren, A. Saeki, S. Yoshikawa, N. M. Murari, S. Subramaniyan, M. J. Crane, S. Seki, S. A. Jenekhe, *J. Am. Chem. Soc.* **2014**, *136*, 14589.

[4] a) D. Mori, H. Benten, H. Ohkita, S. Ito, K Miyake, *ACS Appl. Mater. Interfaces* **2012**, *4*, 3325; b)W. Yu, D. Yang, X. Zhu, X. Wang, G. Tu, D. Fan, J. Zhang, C. Li, *ACS Appl. Mater. Interfaces* **2014**, *6*, 2350; c) W. Li, W. S. C. Roelofs, M. Turbiez, M. M. Wienk, R. A. J. Janssen, *Adv. Mater.* **2014**, *26*, 3304; d) I. H. Jung, W. Y. Lo, J. Jang, W. Chen, D. Zhao, E. S. Landry, L. Lu, D. V. Talapin, L. Yu, *Chem. Mater.* **2014**, *26*, 3450; e) P. P. Khlyabich, A. E. Rudenko, B. Burkhart, B. C. Thompson, *ACS Appl. Mater. Interfaces* **2015**, *7*, 2322.

[5] a) X. Zhan, Z. Tan, B. Domercq, Z. An, X. Zhang, S. Barlow, Y. Li, D. Zhu, B. Kippelen, S. R. Marder, *J. Am. Chem. Soc.* **2007**, *129*, 7246; b)E. Zhou, K. Tajima, C. Yang, K. Hashimoto, *J. Mater. Chem.*

2010, *20*, 2362; c) E. Zhou, J. Cong, Q. Wei, K. Tajima, C. Yang, K. Hashimoto, *Angew. Chem. Int. Ed.* **2011**, *50*, 2799; d) Y. Zhou, T. Kurosawa, W. Ma, Y. Guo, L. Fang, K. Vandewal, Y. Diao, C. Wang, Q. Yan, J. Reinspach, J. Mei, A. L. Appleton, G. I. Koleilat, Y. Gao, S. C. B. Mannsfeld, A. Salleo, H. Ade, D. Zhao, Z. Bao, *Adv. Mater.* **2014**, *26*, 3767; e) W. Liu, R. Tkachov, H. Komber, V. Senkovskyy, M. Schubert, Z. Wei, A. Facchetti, D. Neher, A. Kiriy, *Polym. Chem.* **2014**, *5*, 3404; f) Y. J. Hwang, T. Earmme, B. A. E. Courtright, F. N. Eberle, S. A. Jenekhe, *J. Am. Chem. Soc.* **2015**, *137*, 4424.

[6] a) Y. J. Hwang, G. Ren, N. M. Murari, S. A. Jenekhe, *Macromolecules* **2012**, *45*, 9056; b) T. Earmme, Y. J. Hwang, N. M. Murari, S. Subramaniyan, S. A. Jenekhe, *J. Am. Chem. Soc.* **2013**, *135*, 14960; c) E. Zhou, J. Cong, K. Hashimoto, K. Tajima, *Adv. Mater.* **2013**, *25*, 6991; d) N. Zhou, H. Lin, S. J. Lou, X. Yu, P. Guo, E. F. Manley, S. Loser, P. Hartnett, H. Huang, M. R. Wasielewski, L. X. Chen, R. P. H. Chang, A. Facchetti, T. J. Marks, *Adv. Energy Mater.* **2014**, *4*, 1300785; e) D. Mori, H. Benten, I. Okada, H. Ohkita, S. Ito, *Energy Environ. Sci.* **2014**, *7*, 2939; f) Y. J. Hwang, T. Earmme, S. Subramaniyan, S. A. Jenekhe, *Chem. Cummun.* **2014**, *50*, 10801; g) T. Earmme, Y. J. Hwang, S. Subramaniyan, S. A. Jenekhe, *Adv. Mater.* **2014**, *26*, 6080; h) D. Mori, H. Benten, I. Okada, H. Ohkita, S. Ito, *Adv. Energy Mater.* **2014**, *4*, 1301006; i) H. Kang, K. H. Kim, J. Choi, C. Lee, B. J. Kim, *ACS Macro Lett.* **2014**, *3*, 1009; j) C. Lee, H. Kang, W. Lee, T. Kim, K. H. Kim, H. Y. Woo, C. Wang, B. J. Kim, *Adv. Mater.* **2015**, *27*, 2466.

[7] W. Ma, C. Yang, X. Gong, K. Lee, A. J. Heeger, *Adv. Funct. Mater.* **2005**, *15*, 1617.

[8] B. A. Gregg, *J. Phys. Chem.* **1996**, *100*, 852.

[9] H. Xin, F. S. Kim, S. A. Jenekhe, *J. Am. Chem. Soc.* **2008**, *130*, 5424.

[10] a) J. Peet, J. Y. Kim, N. E. Coates, W. L. Ma, D. Moses, A. J. Heeger, G. C. Bazan, *Nature Mater.* **2007**, *6*, 497; b) H. Xin, X. Guo, G. Ren, M. D. Watson, S. A. Jenekhe, *Adv. Energy Mater.* **2012**, *2*, 575.

[11] a) J. M. Frost, F. Cheynis, S. M. Tuladhar, J. Nelson, *Nano Lett.* **2006**, *6*, 1674; b) C. R. McNeill, N. C. Greenham, *Adv. Mater.* **2009**, *21*, 3840; c) C. R. McNeill, *Energy Environ. Sci.* **2012**, *5*, 5653; d) M. M. Alam, C. J. Tonzola, S. A. Jenekhe, *Macromolecules*, **2003**, *36*, 6577; e) L. A. Utracki, *Polymer Alloys and Blends*, Hanser Publishers, New York **1990**.

[12] a) C. Cui, W. Y. Wong, Y. Li, *Energy Environ. Sci.* **2014**, *7*, 2276; b) S. H. Liao, H. J. Jhuo, P. N. Yeh, Y. S. Cheng, Y. L. Li, Y. H. Lee, S. Sharma, S. A. Chen, *Sci. Rep.* **2014**, *4*, 6813.

[13] B. C. Thompson, P. P. Khlyabich, B. Burkhart, A. E. Aviles, A. Rudenko, G. V. Shultz, C. F. Ng, L. B. Mangubat, *Green*, **2011**, *1*, 29.

[14] S. A. Jenekhe, L. Lu, M. M. Alam, *Macromolecules* **2001**, *34*, 7315.

[15] G. Ren, C. W. Schlenker, E. Ahmed, S. Subramaniyan, S. Olthof, A. Kahn, D. S. Ginger, S. A. Jenekhe, *Adv. Funct. Mater.* **2013**, *10*, 1238.

[16] P. Schilinsky, C. Waldauf, C. J. Brabec, *Appl. Phys. Lett.* **2002**, *81*, 3885.

[17] L. M. Andersson, C. Muller, B. H. Badada, F. Zhang, U. Wurfel, O. Inganas, *J. Appl. Phys.* **2011**, *110*, 024509.

[18] A. L. Patterson, *Phys. Rev.* **1939**, *56*, 978.

[19] N. M. Murari, M. J. Crane, T. Earmme, Y. J. Hwang, S. A. Jenekhe, *Appl. Phys. Lett.* **2014**, *104*, 223906.